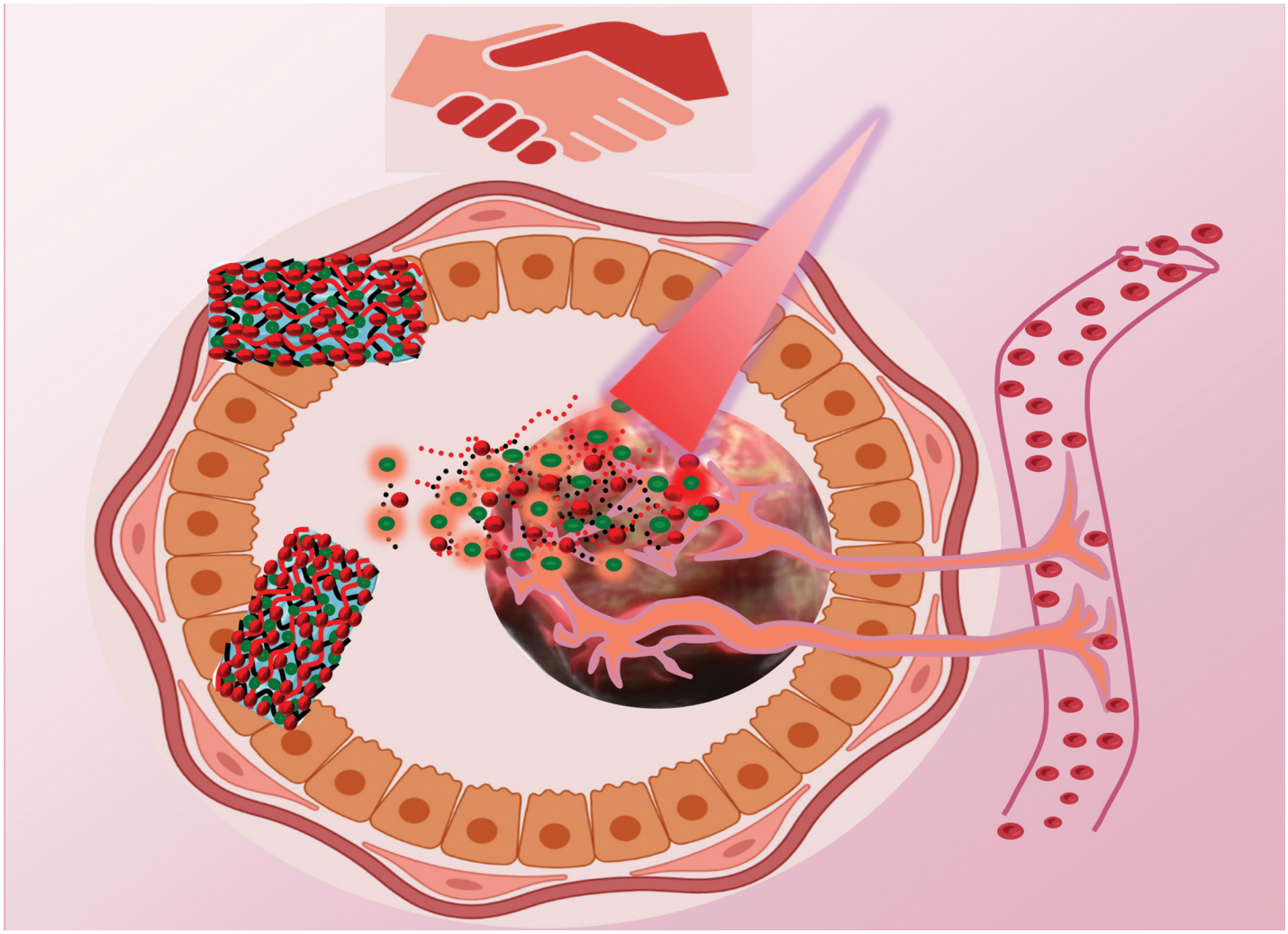

Showcasing research from Dr Jayeeta Bhaumik's laboratory, Department of Nanomaterials and Application Technology, Center of Innovative and Applied Bioprocessing, Punjab, India

A photoarchitectonic hydrogel for synergistic *in vitro* chemo–phototherapy of breast cancer

Preparation of Doxorubicin (Dox) conjugated on carbon dots and zinc phthalocyanine (ZnPc) incorporated hydrogel using PEGMA and PAA polymer was accomplished. The combinatorial chemo-phototherapeutic hydrogel is capable of releasing chemo and phototherapeutic drugs (Dox and ZnPc) in response to pH and emits reactive oxygen species when exposed to laser light at the breast cancer cell location. This research outcome indicates that the photoarchitectonic hydrogel has the potential to undergo synergistic chemo- and photodynamic therapy for cancer treatment.

As featured in:

See Jayeeta Bhaumik *et al.*, *Mater. Adv.*, 2024, **5**, 1903.

ROYAL SOCIETY OF CHEMISTRY

rsc.li/materials-advances

Registered charity number: 207890

Materials Advances

ROYAL SOCIETY OF CHEMISTRY

PAPER

View Article Online
View Journal | View Issue

Cite this: *Mater. Adv.*, 2024, 5, 1903

A photoarchitectonic hydrogel for synergistic *in vitro* chemo–phototherapy of breast cancer†

Shatabdi Paul,[ab] Binduma Yadav,[bc] Mahesh D. Patil,‡[a] Anil Kumar Pujari,[ad] Umesh Singh,[a] Vikas Rishi[c] and Jayeeta Bhaumik *[ab]

Currently, combinatorial therapy has evoked interest in cancer treatment, and may promote achieving a synergistic effect using cancer medicines. Laser-assisted and pH-responsive therapies have attracted significant attention, and their combination leads to high efficiency cancer treatment. Herein, we developed a chemo–phototherapeutic hydrogel comprised of doxorubicin (DOX, a chemotherapeutic drug) and zinc phthalocyanine (ZnPc, a phototherapeutic drug) for combinatorial and synergistic treatment of breast cancer. Firstly, we have developed carbon dots (CDs, size of ~5 nm) utilizing lignin and folic acid as biocompatible sources. Then doxorubicin was loaded on the surface of the carbon dots *via* conjugation (DOX@CDs). Later on, zinc phthalocyanine and acrylic acid derivatives were utilized to develop a laser-responsive hydrogel (ZnPc-PP H). Afterward, doxorubicin-conjugated carbon dots were incorporated into the photoarchitectonic hydrogel to develop a chemo–phototherapeutic drug-loaded hydrogel (DOX@CDs–ZnPc-PP H). Subsequently, the *in vitro* pH-triggering experiments demonstrated that the hydrogel loaded with both DOX and ZnPc could release the drugs in an acidic environment. Interestingly, *in vitro* assays confirmed that DOX@CDs–ZnPc-PP H could effectively target breast cancer cells (MCF-7). Furthermore, the developed chemo–phototherapeutic hydrogel exhibited non-cytotoxic behavior. Owing to laser assisted reactive oxygen species generation from ZnPc present in the hydrogel, the growth of MCF-7 cells was significantly lowered. In conclusion, all experimental outcomes indicate that the photoarchitectonic hydrogel has the potential to be applied in synergistic chemo- and photodynamic therapy of cancer.

Received 24th October 2023,
Accepted 20th December 2023

DOI: 10.1039/d3ma00900a

rsc.li/materials-advances

Introduction

Cancer is a congenital disorder with a high death rate and is defined by aberrant cell development, proliferation, and metastasis.[1] Breast cancer is the second foremost reason of cancer deaths in women in the United States, followed by lung cancer.[2] Over the last 50 years, breast cancer has been the most significant cause of mortality in women globally, with an estimated 1 in 9 women being diagnosed with it at some point of time.[3] Rapid sociological, economic, and lifestyle changes are responsible for this worldwide trend in breast cancer among women, and have resulted in a consistent rise in occurrence (25%) and mortality (15%) rates, respectively.[4] Furthermore, despite the clinical availability of numerous antitumor treatment techniques, including radiotherapy, surgery, and chemotherapy, breast cancer remains one of the fatal diseases worldwide.[5]

Doxorubicin (DOX) is a prominent cancer chemotherapeutic drug used to treat many types of carcinomas and soft tissue sarcomas.[6] Like most anticancer chemotherapeutic drugs, DOX has systemic adverse effects because of the non-selective uptake of the drug by healthy non-cancerous tissues. The recent research efforts aim to improve the efficacy and selectivity of targeted drug delivery systems, which can selectively transport and release drugs at cancer sites.[7,8] Next, to deliver chemotherapeutic drugs to tumor areas, nanoparticles are used.[9] Recent developments in receptor-mediated targeted drug delivery methods using different targeting ligands, such as folic acid (FA), are noteworthy.[10] Folic acid receptor-mediated uptake by

[a] *Center of Innovative and Applied Bioprocessing (CIAB), Department of Nanomaterials and Application Technology, Department of Biotechnology (DBT), Government of India, Sector 81 (Knowledge City), S.A.S. Nagar, 140306, Punjab, India. E-mail: jayeeta@ciab.res.in*
[b] *Regional Centre for Biotechnology, Department of Biotechnology (DBT), Government of India, Faridabad 121001, Haryana, India*
[c] *National Agri-Food Biotechnology Institute (NABI), Department of Biotechnology (DBT), Government of India, Sector 81 (Knowledge City), S.A.S. Nagar, 140306, Punjab, India*
[d] *Department of Chemical Sciences, Indian Institute of Science Education and Research, Sector-81 (Knowledge City), S.A.S. Nagar, 140306, Mohali, Punjab, India*

† Electronic supplementary information (ESI) available. See DOI: https://doi.org/10.1039/d3ma00900a

‡ Present address: Chemical Engineering & Process Development Division, CSIR-National Chemical Laboratory, Dr Homi Bhabha Road, Pune 411008, India.

endocytosis might be applied for drug delivery systems. In this context, carbon dots (CDs) that exhibit excellent biocompatibility, strong surface functionality, and improved cellular absorption have become potential drug delivery carriers.[11,12] Extensive studies have been carried out on the preparation of CDs, and several approaches, including hydrothermal cracking, microwave-mediated synthesis, and oxidation of carbon nanotubes and graphite, have been developed.[13] Hydrothermal methods have been the most extensively used of these techniques because they are easy to use and economically friendly, and they can be carried out under controlled reaction conditions.[14] Recently, enhanced cellular absorption, strong surface activity, and outstanding biocompatibility make CDs an attractive alternative for improving the effectiveness of cancer treatment and reducing adverse side effects. Due to the prevalence of numerous functional groups, including NH_2, OH, and COOH, that are present on the surface of CDs, it is feasible for CDs to interact with various drugs through covalent or electrostatic bonding.[15] In this context, research has demonstrated that DOX conjugated carbon dots, compared to only DOX, are more effective in targeting cells, probably owing to the high receptor-mediated transport to the cancer sites.[6,9] Hence, chemotherapeutic drug conjugated carbon dots would pave the way to deliver the drugs to the cancer sites.

According to recent studies, combinatorial therapy can activate many cytotoxic pathways,[16] resulting in a synergistic antitumor effect. Recently, using multimodal therapeutic nanomaterials in combinatorial cancer treatment has attracted interest.[17] Combinational use of drugs has lately become a smart strategy to treat a complicated disease. The benefits of the combinational use of drugs include synergistic effects, low toxicity, dosage reduction, and reduced drug resistance.[18–20] Combining targeted delivery systems, chemotherapy, and photodynamic therapy (PDT) result in effective cancer treatment.[16,21] As a result, PDT in combination with chemotherapy has gained enormous interest in cancer therapy. Also, the combination of PDT and chemotherapy can improve the therapeutic efficacy of low-dose chemotherapy and thereby reduce the side effects and drug resistance.[22–24] Furthermore, to avoid unwanted cytotoxicity, chemotherapeutic agents should be released in a controlled manner. Among the several stimuli, using a photosensitization process to produce reactive oxygen species (ROS) has attracted the most attention.[25–27]

In this context, using red laser capable of penetrating several centimeters into human soft tissue with minimal damage is a non-invasive external approach.[28] Photodynamic therapy (PDT) is a photochemical approach in which a photosensitizer is applied that causes localized tumor tissue damage when the tissue is exposed to light.[29,30] ROS, particularly singlet oxygen, are generated by the combined action of three individually nontoxic elements, including a photosensitizer, light with a particular wavelength, and oxygen, to cause cellular and tissue damage.[31] Zinc phthalocyanine (ZnPc), a food and drug administration (FDA), USA-approved photosensitizer activatable by red laser, has been proven to be successful in treating cancers.[32] Zinc phthalocyanine (ZnPc)-mediated photodynamic therapy (PDT) is effective as a unique therapeutic method in treating breast cancer *in vitro*.[33,34] Owing to their strong absorption in the phototherapeutic window (650–800 nm) and high efficiency in generating ROS, zinc(II) phthalocyanines, second-generation photosensitizers for PDT, are highly promising imaging agents. Notably, phthalocyanine, one of the zinc(II) phthalocyanine derivatives, is currently undergoing phase II clinical trials to treat MCF-7 tumors.[33] Light-responsive drugs, *i.e.*, hydrophobic phthalocyanine macrocycles, could coordinate with a hydrophilic polymer to form a ZnPc–polymer-based hydrogel.

Furthermore, pH is important in most biological and many chemical systems. Precise monitoring of the physiological pH is highly recommended for treating various pathological and physiological conditions.[35] A slight alteration in pH may indicate serious health issues, including cancer. Therefore, pH-responsive hydrogels are emerging as drug carriers to achieve the localized and site-specific sustained release of drugs in breast cancer.[31,36,37] They have some significant features like possessing softness and resemblance to biological systems. Hydrogels have drawn a great deal of interest with a wide range of possible medical, pharmacological, and prosthetic uses.[38,39] Hydrogels are three-dimensional hydrophilic polymer networks that hold a significant fraction of water.[40] Hydrogels have capacity to absorb water and their swelling and permeability characteristics facilitate their direct biological use. These traits result in their rapid solubilization under pH stimuli, and their structure's weak mechanical strength allows them to undergo structural deformations.[41,42] The crosslink density and distribution of a hydrogel network impact its mechanical properties, as structural heterogeneity may enhance its mechanical strength.[43] Recent research on hydrogels has shown that two independently crosslinked biocompatible polymer networks can increase their mechanical strength. Therefore, two types of polymers have been considered, namely, poly(ethylene glycol) (PEG) and poly(acrylic acid) (PAA), where these two polymers were crosslinked to form a hydrogel.[43] Non-linear PEG analogs, particularly PEGMA, are recognized to be biocompatible similar to linear PEG.[44] Incorporating multifunctional nanoparticles into a hydrogel can produce an effective and smart delivery system. Therefore, incorporating nanoparticles into pH-responsive hydrogels, such as carbon dots (CDs), may result in an assembly with increased mechanical properties.

Various stimuli-responsive hydrogels have been developed for 'smart' drug delivery.[45,46] Although hydrogels and carbon dots are independently studied for drug delivery, no reports on integrating hydrogels and carbon dots to target cancer cells are available. Furthermore, combinatorial drugs to be administered can be enclosed in a hydrogel and delivered at tumor sites maintaining a high drug concentration in the tumor tissue for an extended period and lessening systemic toxic side effects.[47] Therefore, our research focuses on developing a ZnPc-based hydrogel system using a biocompatible polymer. Initially, an integrated DOX conjugated CDs and ZnPc-PP hydrogel system was developed. The resulting chemo–phototherapeutic

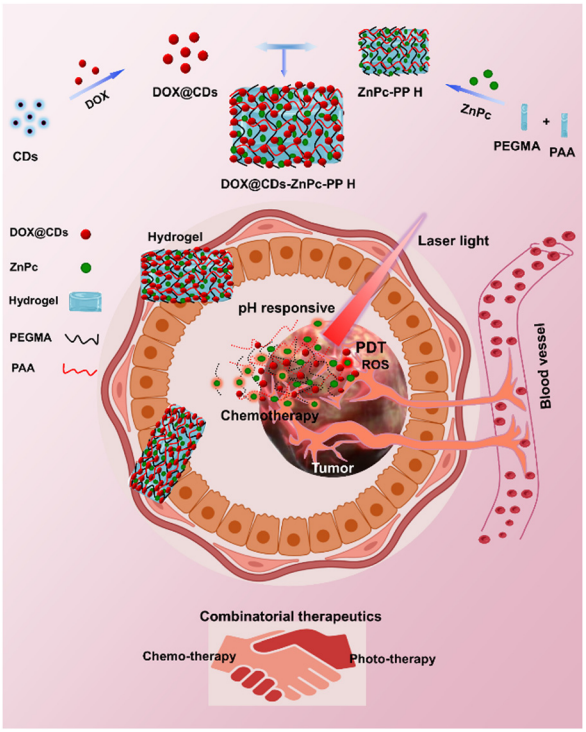

Scheme 1 Schematic illustration of the preparation of doxorubicin (Dox) conjugated CDs (Dox@CDs) and a zinc phthalocyanine incorporated hydrogel using PEGMA and PAA polymers (Top part of the scheme). (b) The combinatorial chemo–phototherapeutic hydrogel releases drugs in response to pH and generates reactive oxygen species when exposed to laser light at the breast cancer cell location (Bottom part of the scheme).

drug-loaded hydrogel system was utilized in red laser assisted drug delivery which released the therapeutic drugs in the cancer microenvironment. We demonstrate that DOX@CDs–ZnPc-PP H with a combinatorial dose of the chemo–phototherapy drugs elicits anticancer efficacy after a single treatment. Therefore, red laser assisted ROS-generation by the photoarchitectonic hydrogel with combined chemo–phototherapeutic drugs can be applied to destroy breast cancer cells as illustrated in Scheme 1. Finally, the cell viability assessment was conducted for the Michigan Cancer Foundation (MCF-7) breast cancer cell line to evaluate the anticancer potential of the material.

Results and discussion

Preparation and characterization of carbon dots and chemotherapeutic drug-conjugated carbon dots

Over the past few decades, non-cytotoxic carbon dots (CDs) have emerged as the formulation for targeted drug delivery.[48] Drug composites were developed by simply mixing many different therapeutic agents with carbon dots (CDs) as cargoes for cancer therapies. Therefore, the drug's addition order and the reactants' concentration were optimized in the present study. CDs were synthesized using lignin and folate receptor-targeted moieties, *viz.* folic acid, to form a solution, following which the

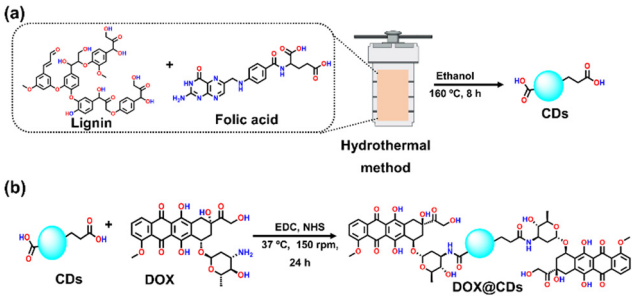

Scheme 2 Schematic illustration of the carbon dots (CDs) (a) synthesis from lignin and folic acid as a coating *via* a hydrothermal method and (b) the conjugation of doxorubicin (DOX) on CDs (DOX@CDs).

chemotherapeutic agent DOX was conjugated. As illustrated in Scheme 2(a), kraft lignin (a biocompatible polymer) and folic acid were used as the precursors for the simple one-pot hydrothermal method-based synthesis of kraft lignin and folic acid functionalized carbon dots (CDs). Briefly, the CDs were synthesized by the hydrothermal treatment of varying ratios of lignin and folic acid in ethanol at temperatures ranging from 100–200 °C for 2–10 h. The resultant CD solutions were assessed for size and surface charge. The optimal CD solution was obtained with a weight ratio of lignin : folic acid at 2 : 1 (% w/w), and it displayed a surface charge of −22.12 mV at pH 7.0 (ESI,† Section S2 and Fig. S1).

The high-resolution transmission electron microscopy (HR-TEM) images of CDs displayed black dots with an average size of ∼4.6 nm (Fig. 1(a)–(c)). The HR-TEM images also showed visible lattice fringes (Fig. 1(d)), which corresponded to the *d*-spacing of the carbon planes, with a lattice spacing of 0.21 nm (Fig. 1(e)). The standard atomic configurations seen in most CDs suggested a high degree of crystallinity.[49] In this line, the crystalline character of the material is well demonstrated by the bright spots in the selected area electron diffraction (SAED) pattern (Fig. 1(e)). A broad single diffraction peak in the XRD pattern centred at angle of 25° is attributed to disordered carbon atoms with an amorphous surface structure (Fig. 1(f)).[50,51] Furthermore, the analysis of the composition of CDs using EDS (energy-dispersive X-ray spectroscopy) revealed the uniform distribution of C, O, and N. The presence of N and C elements of the folic acid showed its successful embedding on the CDs (Fig. S2 and Table S1, ESI†).

Next, the UV-Vis absorption and FTIR spectra of the CDs were obtained to examine the assembly of the lignin–folic acid-based CDs. The CDs are developed *via* π–π stacking interactions, and their peaks are observed at 212 nm and 264 nm (Fig. 1(g)).[52] Additionally, the FTIR spectra were used to confirm the formation of CDs (Fig. 1(h)). Importantly, a C═O (acid) stretching frequency peak was observed in the fingerprint area in the range of 1750–1600 cm^{-1} and a broad absorption peak in the range of 3500–3000 cm^{-1} due to the –OH and $–NH_2$ functional groups of folic acid which is retained in CDs. A similar FTIR pattern has been reported for CDs prepared hydrothermally from citric acid and ethylenediamine.[39] Next, in the XRD pattern of the crystalline phase of CDs, peaks were

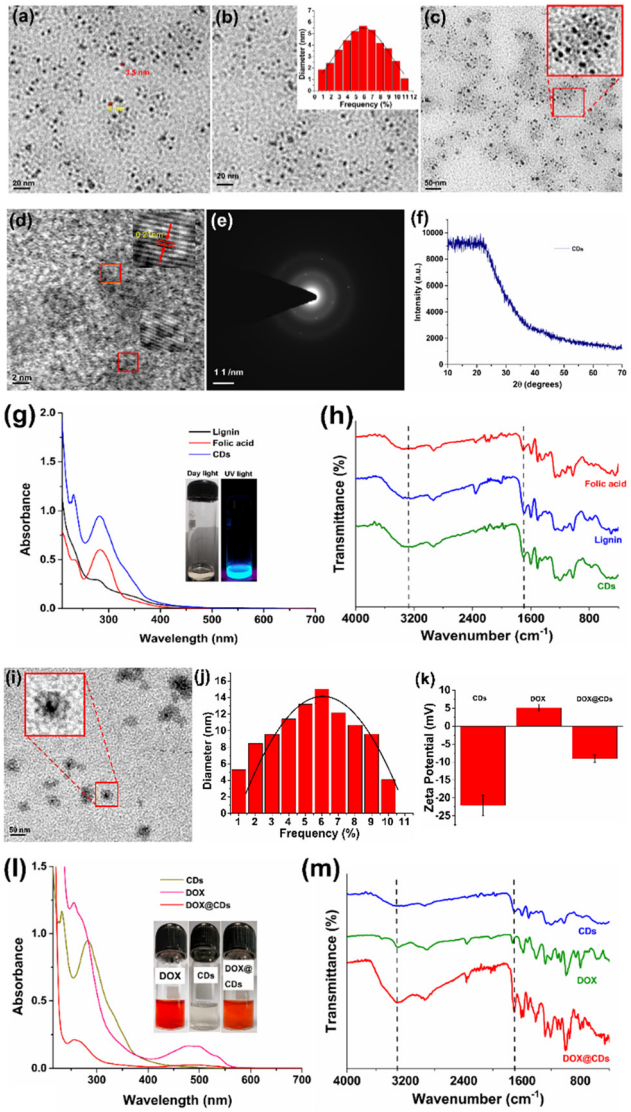

Fig. 1 (a)–(d) High-resolution electron microscopy images of CDs. (e) SEAD pattern of only CDs. (f) XRD pattern of CDs. (g) UV-Vis spectra (h) FTIR spectra. (i) High-resolution electron microscopy images of DOX conjugated CDs (DOX@CDs). (j) Average particle size of DOX conjugated CDs and (k) zeta-potential of CDs and DOX and DOX@CDs. (l) UV-Vis spectra of CDs, DOX, and DOX@CDs. (m) FTIR spectra of DOX@CDs and DOX.

observed at 11.08, 26.92, and 28.5 (Fig. 1(f)). However, lignin depicts amorphous nature (Fig. S3, ESI†). However, peaks present at 2θ of 11.12, 14.2, 16.1, 23.8, 27.1, and 28.5° with a slight shift for the CDs can be attributed to the formation of a folic acid layer and they were compared with the reported folic acid peaks[40] for confirming that the lignin–folic acid carbon dot synthesis was accomplished.

Subsequently, to improve the targeted delivery of DOX, it was conjugated with the surface of CDs (DOX@CDs) using EDC–NHS coupling. For this, the conjugation reaction was carried out using the CDs. The carboxylic group of folic acid on the CDs can be coupled to the NH_2 group of DOX to form an amide linkage between CDs and DOX as shown in Scheme 2(b). In a typical reaction, CDs (10 mL, 1 mg mL^{-1} water) and a solution of DOX (1 mL, 1 mg mL^{-1}) were coupled. To activate the carboxylic acid group of CDs, aqueous solutions of the coupling reagent EDC (80 μL, 5 mg mL^{-1}) and after some time NHS (80 μL, 5 mg mL^{-1}) were added to generate a highly active ester center that was responsible for DOX conjugation. The reaction mixture was then agitated in the dark for 24 hours at a temperature of 37 °C and 150 rpm. Following the centrifugation and decantation procedures, DOX@CDS was purified (washing three times, 16 000 rpm, 20 min). Furthermore, HR-TEM images confirmed the successful conjugation of DOX on the CDs, and the size of spherical-shaped DOX@CDs was ∼12 nm (Fig. 1(i)). The average particle size obtained for the distributed DOX conjugated CDs (DOX@CDs) displayed that the maximum size of nanoparticles was on the order of 12 nm (Fig. 1(j)); the zeta potential (ζ) values of the CDs and DOX@CDs were −22.12 mV and −9.03 mV, respectively (Fig. 1(k)). The decrease in the surface charge suggested that the conjugation of DOX on the surface of CDs was accomplished. The drug loading percentage of DOX@CDs was calculated to be 65 ± 1.2% (Table S2 and Fig. S4, S5, ESI†) using the standard plot of only DOX (Fig. S4, ESI†). UV-Vis absorption spectra revealed the red-shifting of the characteristic peak of DOX from 480 to 500 nm, corroborating the conjugation of DOX on CDs (Fig. 1(l)).

Next, the FTIR spectra of DOX@CDs revealed a distinctive intense absorption peak at 1800–1600 cm^{-1} with a significant shift that was attributed to the –CONH stretching vibrations of the amide linkage between CDs and DOX (Fig. 1(m)). The broad stretching peaks at 3500–3000 cm^{-1} were ascribed to $-NH_2$ and –OH functional groups present in DOX and CDs. Also, the FTIR spectrum of DOX@CDs reflects that the the conjugation of DOX onto the surface of CDs was successfully achieved (Fig. 1(h)). In addition, the crystal structure of DOX@CDs was investigated by X-ray diffraction (XRD). In the case of only DOX, a clear crystalline phase was seen in its native phase. Nevertheless, the lowest degree of crystallinity was observed in DOX@CDs (Fig. S6, ESI†).

Fabrication and characterization of phototherapeutic drug-loaded hydrogels (ZnPc-PP H)

Zinc(II)phthalocyanine (ZnPc) has emerged as an effective red light-responsive drug in PDT, owing to its distinct features such as strong photo-stability and its potential to convert visible excitation photons to reactive singlet oxygen species.[53] However, the applicability of ZnPc with photophysical characteristics in a biological microenvironment is confined due to some limitations, including low water solubility, colloidal stability, and a lack of selectivity for cancer cells.[31] Therefore, researchers have tried to integrate ZnPc into a carrier system to increase its therapeutic efficiency while minimizing its limitations.[54] Stimuli-responsive hydrogels are cross-linked polymer networks that have received significant interest. Owing to their exceptional virtues, namely, high-water content, tuneable pore size and surface area as well as absorption ability of drugs, they show good tumor targeting ability, prolonged blood circulation,

excellent biocompatibility, and slow and sustained release of drugs.[45]

To endow ZnPc with laser-induced therapeutic ability, hydrogels were developed for pH-responsive sustained release of drugs. For this purpose, hydrogels were fabricated using biocompatible polymers PEGMA [poly(polyethylene glycol methyl ether methacrylate)] and PAA (polyacrylic acid) and zinc phthalocyanine using a chemical cross-linking reaction. Consequently, the weight ratio of PEGMA : ZnPC : PAA was optimized (ESI,† Fig. S7). As shown in Scheme 3, the synthesized zinc phthalocyanine–poly(polyethylene glycol methyl ether methacrylate–polyacrylic acid) hydrogel (ZnPc-PP H) is a cross linked hydrogel with the ZnPc photosensitizer bonded between PEGMA and PAA. The light-responsiveness of drug ZnPcs allows it to interact with the PEGMA[55] and PAA[56] hydrogel *via* hydrogen bonding and co-ordination interactions.[57] Potassium persulfate (KPS) has been introduced as a free radical initiator for cross-linking of PEGMA and PAA. Hence, ZnPc-PP H was developed upon step-wise addition of all the mentioned reagents under heating conditions (at 70 °C for 30 min). Transparency is the foremost requirement for photodynamic treatment because it allows light to pass through a hydrogel and excite a photosensitizer.[35] Consequently, the transmittance of the newly developed hydrogel was recorded in the 200 to 700 nm wavelength range. ZnPc-PP H under red laser irradiation and the transmittance of red laser at different concentrations of ZnPc in the developed hydrogel of (i) 0.071 wt/vol%, (ii) 0.14 wt/vol%, (iii) 0.21 wt/vol%, (iv) 0.28 wt/vol%, and (v) 0.35 wt/vol% are illustrated in Fig. 2(a). This figure indicates that typically 5 mg of ZnPc-PP H would be effective for laser light-induced anticancer therapy. Further validation was done by measuring transmittance at different concentrations of ZnPc in the hydrogel. The results showed that 5 mg concentration of ZnPc in the hydrogel exhibited 90% of transmittance compared to 10, 15, 20, and 25 mg ZnPc (Fig. 2(b)).

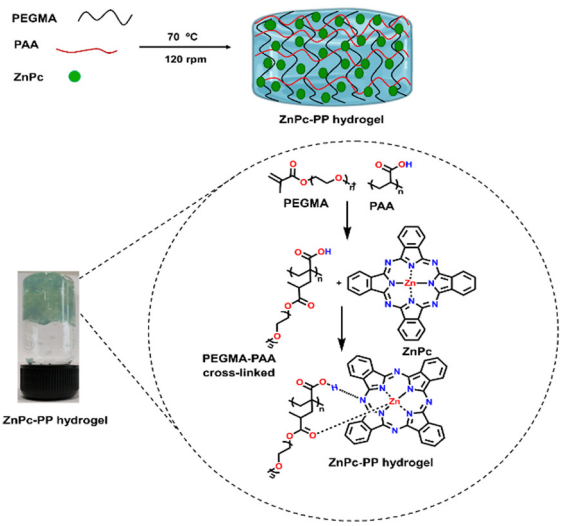

Scheme 3 Schematic illustration of fabrication of a pH-responsive combinatorial chemo–phototherapeutic hydrogel.

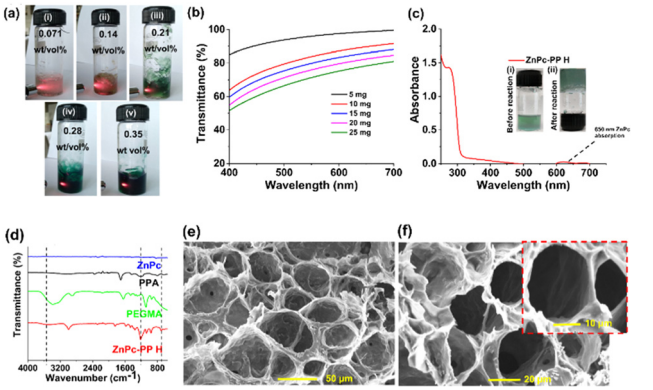

Fig. 2 (a) Pictorial representation of ZnPc-PP H; red laser transmitted at different concentrations of ZnPc in the developed hydrogel: (i) 0.071 wt/vol%, (ii) 0.14 wt/vol%, (iii) 0.21 wt/vol%, (iv) 0.28 wt/vol%, and (v) 0.35 wt/vol% facilitating its anticancer activity. (b) Transmittance analysis of different weight% of hydrogels. (c) UV-Vis spectrum of ZnPc-PP H; the inset image represents (i) before reaction (0.071 wt/vol%) and (ii) after reaction (0.071 wt/vol%). (d) FTIR spectra of ZnPc-PP H, PEGMA, PAA, and ZnPc. (e) and (f) Scanning electron microscopy (SEM) images of ZnPc-PP H at a scale of 50 μm, 20 μm, and 10 μm (inset: the image of ZnPc-PP H).

Additionally, the UV-Vis absorption spectrum of ZnPc-PP H revealed the characteristic absorption peaks of ZnPc at ~650 nm, PEGMA at ~260 nm, and PAA at ~340 nm. Furthermore, the formation of ZnPc-PP H was confirmed *via* a peak attributed to hydrogen bond and co-ordination interactions between PEGMA and PAA (Fig. 2(c)).[53] Next, FTIR spectroscopy was employed to characterize ZnPC-PP H as shown in Fig. 2(d). The absorption peak at 700–500 cm^{-1} indicated the co-ordination of zinc with the oxygen atom present in the hydrogel. Also, a broad and slightly shifted absorption peak was observed at 1200–1000 cm^{-1} which confirms the hydrogen bond formation between the hydrogel and ZnPc. Additionally, the FTIR spectra of PEGMA and PAA were obtained, in which an ester (–C═O) stretching peak was observed at 1750–1600 cm^{-1} attributing to PEGMA. An acid (–C═O) stretching peak at 1700–1650 cm^{-1} and a stretching peak at 3400–3000 cm^{-1} were observed and were attributed to the –OH functional group present in PAA. The reduction of –OH peak intensity was observed which confirms the hydrogen bonding of ZnPc with the hydrogel (Fig. 2(d)).

Furthermore, energy-dispersive X-ray spectroscopy (EDS) analysis confirmed the presence of the carbon, oxygen, and zinc elements (Fig. S8, ESI†). The presence of Zn, C, and O elements in the hydrogel indicates the presence of ZnPC, PEGMA, and PAA, respectively. The diffraction peaks positioned at 19°, 23.8°, 26.3°, and 28.5° in the XRD pattern may be attributed to the crystalline plane of ZnPc-PP H (Fig. S9, ESI†). The diffraction peaks of PEGMA at 23.3° and ZnPc (23.8°) indicate that the hydrogen and coordination interactions of ZnPc with PEGMA and PAA might decline due to the crystallinity of ZnPc-PP H. The peaks observed at 6.2°, 9.3°, 10.5°, 12.7°, 14.1°, 15.3°, 18.2°, 18.8°, 23.8°, 26.3°, 28.5°, and 30.5° confirmed the presence of ZnPc in the hydrogel.[58] Furthermore, a peak with a 2θ value of 18.5 indicated the decline in

crystallinity due to the grafting of polyacrylic acid onto the PEGMA chain.[59,60] Moreover, the porous network structure of ZnPc-PP H (~200 nm) was investigated using scanning electron microscopy (SEM) analysis (Fig. 2(e) and (f)). The 3D porous network could contribute to the fast adsorption of drugs, which is suitable for the pH-responsive slow and sustained release of drugs from the hydrogel.

Development of chemo–phototherapeutic drug-loaded hydrogels and their characterization

To develop combinatorial chemo–photo therapeutic hydrogels for cancer treatment, we have synthesized DOX@CDs incorporated ZnPc-PP H for efficient tumor treatment, which is a promising candidate for further clinical applications.[45]

To achieve the pH-triggered sustained release of a chemo–photodynamic therapeutic drug in breast cancer cells, DOX@CDs-loaded ZnPc-PP H was developed using a physical absorption approach, as displayed in Scheme 4. DOX@CDs incorporated ZnPc-PP H for dual drug delivery was fabricated in one step. To proceed, DOX@CDs–ZnPc-PP H was constructed through the π–π stacking[61] of the aromatic rings of DOX and ZnPc, respectively, present in DOX@CDs and ZnPc-PP H, as depicted in Scheme 4. Briefly, a combinatorial chemo and phototherapeutic hydrogel was constructed. In this, DOX@CDs was made to absorb by the photoresponsive ZnPc-PP H drug at 25 °C for 8 h.

Subsequently, the final combinatorial drug was analyzed by UV-Vis and FTIR spectroscopy as shown in Fig. 3(a) and (b). To integrate DOX conjugated CDs (DOX@CDs) inside ZnPc-PP H, lyophilized ZnPc-PP H was incubated with the solutions of DOX@CDs until they were completely absorbed by the hydrogel. Furthermore, the UV-Vis absorption spectra of DOX@CDs in ZnPc-PP H in phosphate-buffered saline (PBS) revealed peaks at 260 nm and 340 nm corresponding to PEGMA and CDs, respectively. Next, the two peaks at 490 nm and 650 nm correspond to DOX and ZnPc (Fig. 3(a)). Since ZnPc has an excitation wavelength of 650 nm, herein a red laser was used for photodynamic treatment applications.[31] Subsequently, FTIR spectroscopy was employed for the characterization of DOX@CDs–ZnPC-PP H as shown in Fig. 3(b). DOX@CDs–ZnPc-PP H was fabricated through the π–π stacking of the aromatic rings of DOX and ZnPc, respectively, present in DOX@CDs and ZnPc-PP H. The final formation of the combinatorial hydrogel (DOX@CDs–ZnPc-PP H) was confirmed from the characteristic peaks present in the FTIR spectra. Subsequently, no significant changes were observed in the characteristic peak in the fingerprint print region of the final formulation (DOX@CDs–ZnPcPP H). Notably, the characteristic absorption peaks of DOX@CDs and ZnPC-PP H were retained for the combinatorial hydrogel (Fig. 3(b)).[62] To ensure that the porous structure of ZnPc-PP H was retained upon internalization of DOX@CDs, HR-TEM analysis was performed. It was noticed that DOX@CDs was entirely internalized in ZnPc-PP H, and the size of DOX@CDs was found to be ~12 nm (Fig. 3(c)).

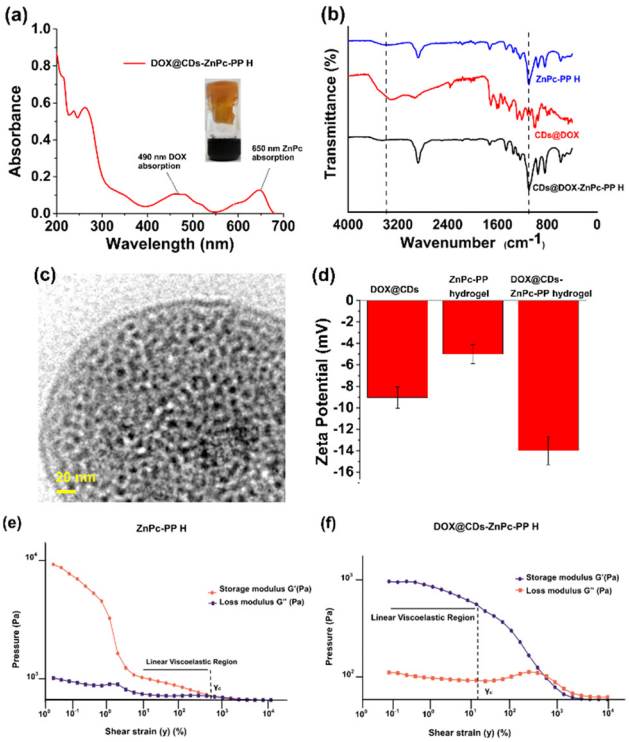

Fig. 3 (a) UV-Vis spectrum of DOX@CDs–ZnPc-PP H. (b) FTIR spectrum of DOX@CDs–ZnPc-PP H. (c) TEM image of DOX@CDs–ZnPc-PP H at a scale of 20 nm. (d) Zeta potential values of DOX@CDs, ZnPc-PP H, and DOX@CDs–ZnPc-PP H. (e) and (f) Rheological measurements of the storage modulus G' and loss modulus G'' of ZnPc-PP H and DOX@CDs–ZnPc-PP H.

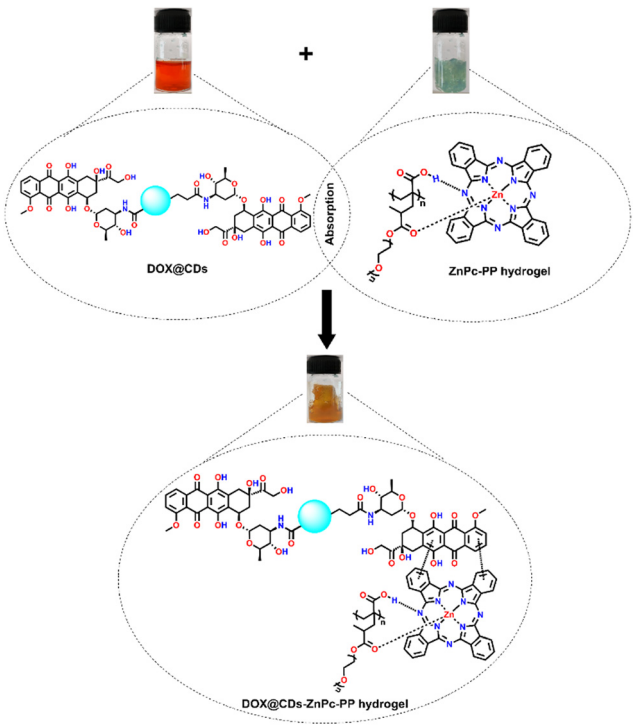

Scheme 4 Construction of final chemo–phototherapeutic drug-loaded hydrogels; absorption of DOX@CDs with ZnPc-PP H.

The absorption of DOX@CDs in the developed hydrogels altered the surface charge (Fig. 3(d)). The resultant surface charge of DOX@CDs–ZnPc-PP H was measured at −14 mV, while the individual surface charges of ZnPc-PP H and DOX@CDs were measured at −5 mV and −9.03 mV, respectively. The swelling percentage of the prepared ZnPc-PP H was 90 wt% (Fig. S7, ESI†). Moreover, the pore size and volume of the hydrogel were studied through N_2 adsorption–desorption isotherms obtained using the multipoint BET technique. The hydrogel showed a multimodal distribution of pores centered at 2.456 nm. Incorporating drugs into the hydrogels strongly led to a decreased pore size of 1.230 nm in agreement with BET data (Fig. S10, ESI†).

Rheological measurements of the chemo–phototherapeutic drug-loaded hydrogels

To better understand the morphology of the developed hydrogel to be a preferable drug carrier, rheological measurements were performed. Moreover, rheology influences storage and loss moduli, viscosity, and flow properties of hydrogels, all of which are important factors to be considered for the use of hydrogels in drug delivery.[40] Viscosity is a key indicator of a material's ability to resist deformation when stress is imposed on it, as well as the potential of a hydrogel to adjust to alterations in shear stress whether it is used *in situ* or *ex situ*.[63] The storage modulus (G') and loss modulus (G'') of hydrogels give adequate information about changes in their elastic and viscous properties in response to oscillatory shear, respectively.[40] These values are essential for studying the behaviour of hydrogels, which is pivotal for delivery of of chemo–phototherapeutic drugs at cancer sites.[40]

The relative elastic and viscous characterization of hydrogels under continuous shear strain has been carried out to determine the linear viscoelastic region in the hydrogel.[64] Higher strain causes the microstructural network of the hydrogel to be disrupted, which causes the stress response to become nonlinear.[40] When DOX@CDs–ZnPc-PP H was subjected to shear strain, it was observed that its γ_c was higher than that of ZnPc-PP H, implying that the mechanical strength of the hydrogel has improved (Fig. 3(e) and (f)). This higher γ_c of DOX@CDs–ZnPc-PP H resulted from the increase in mechanical strength of ZnPc-PP H caused by the absorption of DOX@CDs, as shown in the TEM image (Fig. 3(c)). Reported literature also claimed that the introduction of nanoparticles increased the mechanical strength of a hydrogel which is in accordance with our present study.[63] Furthermore, the continuous flow study results in Fig. S11a and b (ESI†) show that as the shear rate increases, the viscosity of ZnPc-PP H decreases. Meanwhile, DOX@CDs acts as an absorbing agent through the π–π stacking of the aromatic ring between DOX and ZnPc, respectively. Additionally, the presence of DOX@CDs and ZnPc-PP H leads to a more powerful interaction, resulting in a stable hydrogel (Fig. S11a and b, ESI†). The viscosity of both hydrogels was observed to decrease as the shear rate increased, implying that these hydrogels possessed significant shear-thinning capabilities, which enabled them to control the release of therapeutic drugs from them. Fig. S12a and b (ESI†) also show that Zn-PcPP H and DOX@CDs–ZnPc-PP H have larger G' than G'', signifying that they are shear-thinning hydrogel materials.

The viscoelastic behavior of the hydrogel was monitored to instantly observe an alteration in the storage modulus (G') values obtained from the strain/amplitude sweep test of the hydrogel (Fig. S12a and b, ESI†). For around 6000 s at 37 °C, frequency-sweep measurements were performed on the developed hydrogels. For all hydrogels, it was found that the values of G' increase as time increases. Variable angular frequency shear in the range of 0.1–100 rad s^{-1} was applied to the hydrogels at a constant amplitude (1%) in the frequency sweep test. It was observed that the hydrogels exhibited mechanical robustness across all the tested frequency ranges (Fig. S12a and b, ESI†). The higher value of G' than G'' indicates the elastic nature.[40] The hydrogel showed higher values of G' (1311 Pa), which limits its ability to move the chains across the hydrogel matrix. G' values obtained from the frequency sweep test showed a similar trend to those obtained from the amplitude sweep test. Additionally, G' and G'' values of ZnPc-PP H indicate that high-frequency shear forces have disrupted the loose, impermanent ZnPc-PP H network created by either the carboxylic group or the ester group present gradually, demonstrating its propensity towards becoming a liquid, Fig. 3(e). Further, the incorporation of DOX@CDs into ZnPc-PP H significantly improves the mechanical strength of the hydrogel structure through the π–π stacking[61] of the aromatic ring present in the hydrogel (DOX@CDs–ZnPc-PP H) as evidenced by the increase in the LVE region depicted Fig. 3(f). As a result, it is ascertained that ZnPc-PP H and DOX-loaded CDs–ZnPc-PP H are viable solutions for achieving pH-responsive and light-induced cancer treatment. This phenomenon implies that the rheological properties of the prepared hydrogel point to its ease of use as a drug carrier to the cancer sites.

Study of pH responsiveness and stability behavior of the chemo–phototherapeutic drug-loaded hydrogels

The pH-responsive hydrogels hold considerable promise as stimuli-responsive controlled drug delivery vehicles. These hydrogels were evenly segmented into two parts of equal weight and exposed to solutions of acidic and neutral pHs of 5.5 and 7.4 to monitor their pH-triggered behavior. The weight of each of the resulting solutions was then measured at various time intervals (Fig. S13, ESI†). The weight of the hydrogel increased to around 320 mg and remained stable for 20 h in a 7.4 pH PBS buffer. Nevertheless, the weight of ZnPc-PP H maintained at pH 5.5 increased from 220 mg to 280 mg and 340 mg, respectively, then decreased gradually after 20 h.

Furthermore, it was observed that the hydrogels completely disintegrated within 24–72 h as illustrated in Fig. 4(a). This can be attributed to breaking of the H-bonds in the hydrogel at an acidic pH, which ultimately causes the hydrogel to degrade under low pH (5.5) conditions. The drug-incorporated hydrogels, however, exhibited high stability under neutral pH conditions. In conclusion, the developed hydrogel could be used as a

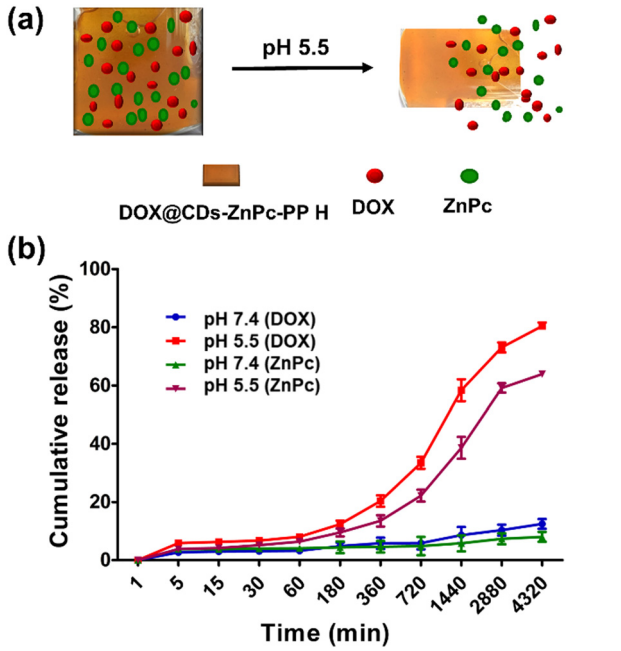

Fig. 4 (a) Schematic illustration of the drug release profile of the combinatorial chemo photo hydrogel (DOX@CDsZnPC-PP H). (b) *In vitro* cumulative release curves of DOX and ZnPc of DOX@CDsZnPC-PP H at pH 7.4 and 5.5.

pH-triggered release material for both therapeutics upon administration under acidic environmental conditions. Following this, a pH-stimuli response study of pH-subjected DOX@CDs–ZnPc-PP H was carried out using SEM (Fig. S14, ESI†). While the pores of the hydrogel were observed to be intact at neutral pH 7, acidic pH disrupted the structure of the hydrogels. The *in vitro* drug release profile was studied using pH-triggered drug release to evaluate the pH responsiveness of the developed hydrogel. Hydrogel development is mainly significant for prolonged nanocarrier-drug release increasing the efficiency of administration and effectiveness of therapeutic drugs delivered to the cancer sites. The benefits of nanocarrier–hydrogel composite materials in drug administration have been demonstrated to be combating the adverse side effects of drugs that, when supplied intravenously, can accumulate in healthy tissues.[65] In this context, our designed drug delivery system was based on the pH-triggered drug release from the hydrogel system. The drug release experiments of DOX@CDs–ZnPC-PP H were carried out at 37 °C and at pHs 7.4 and 5.5. The drug release experiments revealed that DOX@CDs–ZnPC-PP H exhibited strong pH sensitivity (Fig. 4(b)). The cumulative release of DOX at pH 5.5 reached 58.35% within 24 h and 73.07% and 80.43% within 48 h and 72 h, respectively. While the cumulative release of DOX at 24 h, 48 h, and 72 h was 21.62, 23.32, and 26.48%, respectively, in PBS buffer at pH 7.4 (Fig. 4(a) and (b)).

Similarly, the release of ZnPc for 24, 48, and 72 h was found to be 38.62, 59.13, and 63.89%, respectively, at pH 5.5, while it was 5.8, 7.3, and 8.0% for 24, 48, and 72 h, respectively, in PBS at pH 7.4 (Fig. 4(b)). Various cumulative release curves demonstrated that under physiological conditions, DOX and ZnPc would not result in premature leakage. Drug release increases when the acidic environment prevails in the microenvironment of the tumor cell, and DOX release under acidic conditions is increased from 24 to 72 h compared to ZnPc. At the same time, prolonged incubation of the hydrogel under acidic conditions causes the disintegration of bonds, as revealed in SEM images (Fig. S14, ESI†). It should be noted that, the hydrogel is developed *via* optimization in such a way that it only gets triggered by a pH change making it a pH-responsive hydrogel. Furthermore, the hydrogel remains intact upon light exposure and does not release the probes until pH is regulated. To validate this, we monitored the *in vitro* release of DOX and ZnPc under 650 nm laser irradiation for 60 min. The light intensity was adjusted to 50 mW with a five-minute exposure time (“ON”), followed by another five-minute exposure time (“OFF”). The absorption spectra of ZnPc at 650 nm and DOX at 480 nm depicted no significant change under red laser irradiation (Fig. S15, ESI†). As shown in Fig. S15 (ESI†), ZnPc and DOX were not released under laser irradiation (650 nm) up to 60 min. However, the pH responsiveness of the hydrogel at acidic pH (5.5) increases, and the release of DOX and ZnPc from the hydrogel, demonstrating that the concentration of DOX and ZnPc increases considerably at acidic pH (Fig. 4(b)), compared to the unaltered concentration when irradiated (Fig. S15, ESI†). A similar finding has also been reported in the literature, where BTZ (bortezomib) was used for drug therapy, however ICG (indocyanine green) wrapped in supramolecular hydrogels was more light stable than free ICG for photodynamic therapy.[66] Hence, the developed therapeutic hydrogel releasing DOX and ZnPc at acidic pH makes it a pH-responsive hydrogel. Thus, it can be concluded that the final drug delivery system DOX@CDs loaded ZnPC-PP H performed pH-sensitivity-triggered drug release efficiently, which avoids the cytotoxicity towards the normal cells.

Photophysical characterization of the chemo–phototherapeutic drug-loaded hydrogels

Singlet oxygen ($^1O_2$) generation has been found to be a significant factor in estimating the effectiveness of molecules towards PDT.[27] Accordingly, exploring the $^1O_2$ production ability of DOX@CDs–ZnPc-PP H seemed vital. Hence, 1,3-diphenylisobenzofuran (DPBF) that could react with $^1O_2$, was used as a detection probe, and the changes in the DPBF absorption curve were directly proportional to the singlet oxygen ($^1O_2$) generation yield (Φ_Δ).[67] Next, the cytotoxic oxidative stress tissue's oxygen facilitates the degradation of the cell membrane of the treated cells.[68] The phototherapeutic efficiency of the developed chemo–phototherapeutic (DOX@CDs–ZnPc-PP H) hydrogel was therefore evaluated directly with the singlet oxygen quantum yield (SOQY, Φ_Δ). The results were compared using zinc phthalocyanine (ZnPc) as the standard photosensitizer.[31] The absorption profile of DPBF in the presence of reactive oxygen species was obtained. To accomplish this, solutions containing only CDs, DOX@CDs, ZnPc-PP H, and DOX@CDs–ZnPc-PP H, as well as DPBF (blank) and ZnPc (standard drug) were exposed to a red laser (650 nm,

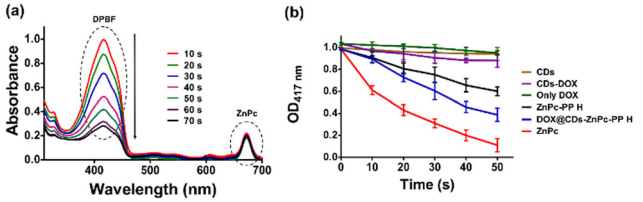

Fig. 5 (a) Graphical illustration of absorption spectra of the DPBF degradation profile treated with DOX@CDs–ZnPc-PP H. (b) Graph displaying the absorption of DPBF solution at 417 nm treated with various probes (CDs, DOX@CDs, only DOX, ZnPc-PP H, and DOX@CDs–ZnPc-PP H, ZnPc) when exposed to 50 mW laser light at different time intervals (0–50 s).

50 mW) for 120 s. The red laser was employed because the excitation wavelength of ZnPc is 650 nm.[31] The DPBF degradation profile facilitates the quantitative analysis of singlet oxygen generation. Subsequently, the reaction product 1,2-dibenzoylbenzene ensures that it does not absorb visible light.[69] Due to the simplicity of reducing the absorption of DPBF, the $^1O_2$ generated by DPBF follows the type II photo mechanism. Fig. 5(a) and (b) show that DOX@CDs–ZnPc-PP H has a significant DPBF absorption decay value (Φ_Δ, 0.81) when compared with different samples, including ZnPc-PP H (Φ_Δ, 0.66) (Fig. 5(b) and Table S3, ESI†). Therefore, ZnPc (Φ_Δ, 0.98) was used as the standard drug.[31] Compared to other probes, including ZnPc alone, ZnPc from the hydrogel induced the generation of ROS with delayed and prolonged release of the phototherapeutic drug (Fig. 5(a)). This confirms that the release through the hydrogel is regulated by diffusion, which might play a vital role in the degradation of the DPBF in the presence of singlet oxygen produced from the photosensitizer.[31] Hence, DOX@CDs–ZnPc-PP H is a valid candidate for PDT.

Laser assisted *in vitro* anticancer efficacy of the chemo–phototherapeutic hydrogel

Chemotherapeutic drugs (DOX) and phototherapeutic drugs (ZnPc) have been extensively used for chemical and laser light-based therapies.[31] Recently, combinatorial therapy, which combines two or more therapeutic drugs, has emerged as a cornerstone of cancer treatment. Owing to its synergistic effects, combinatorial therapy using anticancer drugs shows improved efficacy compared to single-drug therapy.[58] Although combination therapy has shown promising clinical outcomes for the therapy of cancer, this approach is affected by severe systemic adverse drug effects. Therefore, a combinatorial chemo–phototherapeutic hydrogel was fabricated in this study to allow the release of the chemotherapeutic drug doxorubicin (DOX) and phototherapeutic drug ZnPc with controlled release in an acidic environment (Fig. 6(a)). The pH-degradable amide group in DOX@CDs–ZnPc-PP H released the therapeutic drugs in the acidic environment of the breast cancer cells (Fig. 6(b)). The released DOX and ZnPc (which generate ROS in response to red laser) thereby trigger a response to directly kill breast cancer cells.

The present study examined the combinatorial effect of the chemotherapy and phototherapy using DOX@CDs

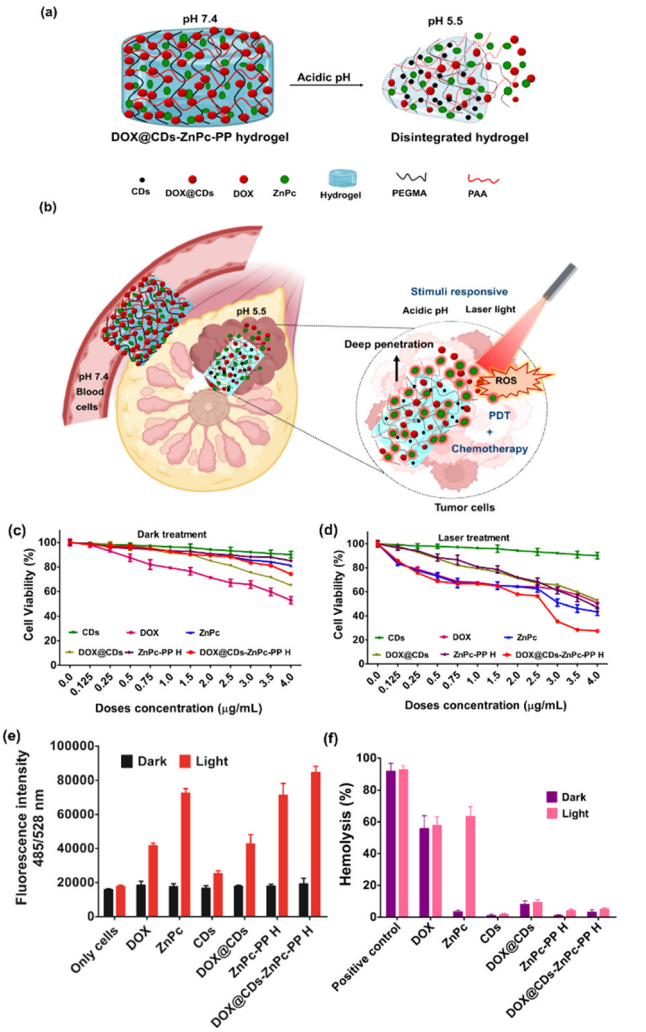

Fig. 6 (a) Schematic diagram of *in vitro* drug releases of DOX and ZnPc from the chemo phototherapeutic hydrogel (DOX@CDs–ZnPc-PP H) under acidic pH. (b) Schematic illustration of pH-responsive drug release and laser-triggered reactive oxygen species generation by the combinatorial chemo–photo therapeutic hydrogel in the breast cancer cell sites. (c) and (d) *In vitro* cell viability of only MCF-7 cells incubated with free CDs, DOX, DOX@CDs, ZnPc, ZnPcPP H, DOX@CDs–ZnPcPP H under the dark and laser conditions (650 nm, 50 mW cm^{-2}, 5 min). Error bars mean ± SD (n = 6). (e) ROS generation studies of untreated MCF-7 cells and treated MCF-7 cells with various samples ($\lambda_{ex}/\lambda_{em}$ = 485/528 nm). (f) *In vitro* hemocompatibility test for the evaluation of compatibility of DOX@CDs–ZnPcPP H; the hemolysis ratio of free CDs, DOX, DOX@CDs, ZnPc, ZnPcPP H, DOX@CDs–ZnPcPP H under the dark and laser conditions. Mean ± SD, n = 3.

incorporated DOX@CDs–ZnPc-PP H. Firstly, the effect of a red laser light intensity (650 nm) on the viability of MCF-7 cells was optimized in the range of 25–100 mW (Fig. S15 and Table S4, ESI†). The cell viabilities obtained upon exposure to 50 mW red laser and those of unexposed control cells (grown in the dark) were 96 and 99%, respectively. This indicates that the exposure to red laser is not toxic to the cell lines as the cell integrity is maintained. Furthermore, the therapeutic efficacy of the combinatorial chemo–phototherapeutic drugs was

Table 1 *In vitro* cytotoxicity IC_{50} of DOX, CDs, ZnPc, DOX@CDs, ZnPc-PP H, and DOX@CDs–ZnPcPP H for MCF-7

S. no.	Probes	IC_{50} (μg mL^{-1}) Dark treatment	Light treatment	Fold of reduction
1.	DOX	10.65 ± 0.10	10.26 ± 0.22	1.03
2.	CDs	20.96 ± 0.20	16.60 ± 0.20	1.26
3.	ZnPc	12.90 ± 0.20	3.17 ± 0.10	4.06
4.	DOX@CDs	8.90 ± 0.20	7.89 ± 0.11	1.12
5.	ZnPcPP H	11.20 ± 0.20	3.82 ± 0.14	2.94
6.	DOX@CDs–ZnPc-PP H	3.65 ± 0.10	1.06 ± 0.18	3.44

investigated using DOX@CDs–ZnPc-PP H, and the results are illustrated in Table 1 and Fig. 6(c), (d). After administration of chemo and phototherapeutic drugs, and irradiation with red laser at 650 nm (50 mW), cells treated with or without CDs remained highly viable.

The IC_{50} values of only DOX and ZnPc for the dark treatment were 10.65 and 12.90 μg mL^{-1}, and those for the laser treatment were found to be 10.26 and 3.17 μg mL^{-1}, respectively. Notably, the chemo–photo therapeutic hydrogel (DOX@CDs–ZnPc-PP H), wherein the combinatorial drugs are loaded, exhibited an IC_{50} value of 3.65 μg mL^{-1} under dark conditions, showing its anticancer potential. However, DOX@CDs–ZnPc-PP H displayed a significant reduction in the cell viability (IC_{50}: 1.06 μg mL^{-1}) upon laser exposure. The treatment under laser irradiation using the chemo–photo therapeutic hydrogel achieved a significant fold reduction (3.44-fold), compared to dark, contributing to the synergistic anticancer effect. Notably, this therapeutic potential of dual drugs can be attributed to various plausible reasons. Firstly, the acidic environment of the MCF-7 cells triggers the release of DOX and ZnPc from the hydrogel. Secondly, DOX, a chemotherapeutic drug, displayed efficient and sustained anticancer ability. Thirdly, the red laser-responsive ZnPc-mediated generation of ROS in the vicinity of cancer cells can also be attributed to the therapeutic effect of the released drugs. Next, combinational use of drugs is a common strategy nowadays. The benefits of combinational use of drugs include synergistic effects, low toxicity, dosage reduction, and reduced drug resistance.[52] As a result, PDT in combination with chemotherapy has aroused enormous interest in cancer therapy. Also, the combination of PDT and chemotherapy can improve the therapeutic efficacy of low-dose chemotherapy and thereby reduce the side effects and drug resistance.[52] To provide more quantifiable information on the dual chemo and photo-therapeutic effect, the combination index (CI) was calculated using the concentration-dependent survival curves. Briefly, in combination therapy, the CI values could be more than 1, equal to 1, or lower than 1 to indicate antagonism, additivity, or synergism, respectively. In the present study, the CI < 1 (the CI value of dark treatment was 0.83 and the CI value of light treatment was found to be 0.84) suggested the synergistic cytotoxic effect owing to the PDT activity of ZnPc and the chemotherapeutic action of DOX at IC_{50} drug concentrations. The obtained value of CI < 1 suggested the synergistic cytotoxic effect exhibited by the combined ZnPc-mediated PDT and DOX-mediated chemotherapy against the MCF-7 cells. Consequently, the findings above demonstrate that DOX@CDs–ZnPc-PP H with a combinatorial dose of chemo–phototherapy drugs elicits anticancer efficacy after a single treatment.

Intracellular ROS generation using the chemo–phototherapeutic hydrogel

Encouraged by the anticancer efficacy of the developed combinatorial chemo–phototherapeutic hydrogel, subsequently, we investigated its intracellular ROS generation ability. For this, the cell-based studies were carried out by treating the MCF-7 cells for 24 h with DOX@CDs–ZnPc-PP H under dark and light conditions and the results obtained were compared with those obtained using other probes (CDs, ZnPc, DOX, DOX@CDs, and ZnPc-PP H). Furthermore, the treated cells were incubated with DCF-DA (2,7-dichlorodihydro fluorescein diacetate) for 1 h, successively.[70] As the non-fluorescent DCFH is oxidized to green fluorescent 2,7-dichlorofluorescein (DCF) in the presence of ROS, the ROS generation was confirmed. Therefore, increased green fluorescence suggests a higher level of ROS production.[71] When treated with chemo–phototherapeutic hydrogel (DOX@CDs–ZnPc-PP H) only under dark conditions, the cells represent a state with low ROS levels (Fig. 6(e)). After exposure to red laser, the cells manifest the highest level of ROS, 4.5 times higher compared to dark treatment [$^{***}p < 0.0001$ (Fig. 6(e))]. However, the fluorescence intensity increased when treated with only ZnPc (4.0 times) and ZnPc-PP H (3.9 times), in contrast to laser and dark treatment. However, a negligible amount of ROS production was observed for only CDs and only DOX and DOX@CDs. Since the above probes are not laser responsive, they result very low levels of ROS production. Laser light responsiveness of the intracellular chemo–phototherapeutic hydrogel elevates the ROS level within the cells. Hence, the foregoing data show that after a single treatment, DOX@CDs–ZnPc-PP H with chemo–phototherapeutic drugs elicits anticancer effectiveness.

Hemocompatibility assay of the chemo–phototherapeutic hydrogel

The potential toxicity concerns of combinatorial chemo–phototherapeutic hydrogels have recently drawn attention due to the advancement of combinatorial-based treatment. In this context, it is imperative to investigate the effects of DOX@CDs–ZnPc-PP H (chemo–phototherapeutic hydrogel) toxicity on blood, in particular erythrocytes as shown in Fig. 6(f). Hemocompatibility of the respective chemo–phototherapeutic hydrogel was investigated by measuring the possible hemolysis percentage when exposed to RBCs, as the chemo–phototherapeutic hydrogel is associated with membrane damage and cell arrest.[72] The hemolysis assay results demonstrate that the chemo–photo combinatorial hydrogel at 3.65 μg mL^{-1} displayed 3% hemolysis under dark conditions and at 1.06 μg mL^{-1} exhibited ~5% hemolysis under laser conditions, which is within the biocompatible range according to ISO/TR 7406, which is the critical safe biomaterial hemolytic ratio

(5%).[72] The current hemolysis assay results revealed blood biocompatibility. The present studies show that DOX@CDs–ZnPc-PP H is biocompatible to erythrocytes, which is contrary to only DOX (~55% hemolysis) and only ZnPc (~60% hemolysis) chemo and photo drugs, respectively. pH-responsive interaction with the RBC membrane (blood pH is 7.4) shows that chemo–photo hydrogel (DOX@CDs–ZnPc-PP H) was intact and there was no release of drugs in the RBC vicinity. However, studies reported that erythrocytes presented significant lysis on incubation with free drugs *i.e.*, DOX and ZnPc, respectively.[73,74] The release of DOX and ZnPc from the hydrogel was induced by acidic pH (5.5) leading to chemotherapeutic and ROS-promoted photodegradation of MCF-7 cells. Though the RBC pH is 7.4 resulting in the intactness of the hydrogel, the hemolytic activity of DOX@CDs–ZnPc-PP H is not observed showing that it is a biocompatible material. This result manifests that the DOX@CDs–ZnPc-PP H only interacted with MCF-7 cells under acidic conditions, thus combinatorial chemo–phototherapy for breast cancer cells is achieved.

Experimental section

Preparation of carbon dots and doxorubicin-conjugated CDs

A mixture of lignin and folic acid was hydrothermally treated to prepare carbon dots (CDs). In brief, lignin (30 mg) and folic acid (15 mg) in a 2 : 1 ratio were mixed in 5 mL ethanol. After that, the mixture was placed into a 30 mL stainless steel autoclave reactor and stirred at 150 rpm for 10 min. The mixture containing vessel was then placed in an oven set at 160 °C, where it was kept for 8 h till reaction completion. It was then allowed to cool to room temperature. Next, to collect the supernatant, the obtained products were centrifuged at 12 000 rpm for 10 min. The supernatant was then re-dispersed in 25 mL of deionized water and subjected to filtration using a nylon-66 membrane syringe filter to obtain homogenous CDs. Later, the CDs were freeze-dried for further conjugation of the anticancer model drug DOX. For this, folic acid-based carbon dots were activated through a EDC/NHS coupling reaction. The solutions of EDC (80 μL, 5 mg mL^{-1}) were added to the carbon dot (CD) solution (10 mg mL^{-1}) and the resulting solution was kept for shaking at 150 rpm for 10 min under the dark conditions to activate the acid groups. Then, NHS (80 μL, 5 mg mL^{-1}) was added to form a highly activated NHS ester, and the reaction mixture was kept on shaking (150 rpm) for 10 min at 37 °C. Subsequently, DOX (1 mg mL^{-1} in water) was added to the reaction mixture and continuously shaken at 37 °C for 24 h. After completion of the reaction, the solution was subjected to centrifugation at 16 000 rpm for 30 min to pelletize the DOX@CDs conjugate. The pellet was resuspended into water (1 mL) and further centrifuged under the same conditions as above to remove unreacted DOX and CDs. The obtained DOX@CDs samples were stored at 4 °C in the dark. Furthermore, the loading percentage of model anticancer drug DOX with CDs in the present drug delivery system was estimated. For this, the supernatant was collected to estimate the drug loading percentage of DOX using a UPLC system. The DOX was eluted isocratically at a 1 mL min^{-1} flow rate using acetonitrile : water (30 : 70) as the eluent and detected using a Waters 2998 PDA detector in the wavelength range 200–800 nm. Notably, the analysis was carried out at 490 nm, at 30 °C, using a reported method while applying some changes.[75] A calibration curve was plotted using varying concentrations of DOX solution to determine the amount of DOX loaded onto the CDs.

$$\text{Loading } \% = \frac{\text{Total drug added} - \text{Drug in the supernatant}}{\text{Total drug added}} \times 100 \quad (1)$$

Fabrication of ZnPc-PP H

To investigate the pH responsive behavior of the hydrogels, poly(ethylene glycol)methyl ether methacrylate (PEGMA), polyacrylic acid (PAA), and zinc-phthalocyanine (ZnPc) were used to synthesize hydrogels. Briefly, 5 mg of ZnPc was dissolved in acetone (500 μL) using bath sonication at room temperature till a transparent solution was obtained. Subsequently, the resulting solution was added over 2 min to a sample of PEGMA (0.3 g) kept at stirring at 150 rpm. Deionized water (7 mL) was added to the resulting reaction mixture. Next, a sample of PAA (75 mg) was added as a cross-linker, followed by the addition of KPS (75 mg) as an initiator of polymerization. The final reaction mixture was heated at 70 °C for 1 h. The reaction mixture was then cooled to room temperature. Thus, an amphiphilic hydrogel was prepared using a chemical cross-linking method. Furthermore, the unreacted materials were removed from the hydrogel by immersing it in deionized water overnight. During washing, no trace of ZnPc was detected in the supernatant as monitored by UV-vis spectroscopy. Hence, the loading percentage of ZnPc into the hydrogel composite was predicted to be ~100%. Finally, the washed ZnPc-PP H was dried to remove excess water and to get the constant weight of hydrogels.

Incorporation of DOX@CDs into ZnPc-PP H

Owing to the three-dimensional network structure of ZnPc-PP H, DOX@CDs can be readily loaded into it. In brief, the synthesized hydrogels were cut into cubes with 1 × 1 × 1 cm dimensions which weighed ~9 mg. The cubes were then immersed into 20 mL of DOX@CDs solution (1 mg mL^{-1}) at room temperature for 24 hours.

Cell culture. The Dulbecco's modified Eagle's medium (DMEM) with 10% fetal bovine serum and 1% antibiotics (penicillin and streptomycin) was applied for culturing breast cancer (MCF 7, acquired from NCCS, Pune, India) cells in a humid atmosphere with 5% CO_2 at 37 °C.

Cytotoxicity assay of the developed probes. The cytotoxicity of different probes was evaluated using the MTT assay. First, 5 × 10^3 MCF7 cells were seeded in 96-well plates. After being seeded in 96 well plates, each well was added with 100 μL fresh media containing different concentrations of probes. After culturing for another 24 h under the dark conditions, the media were replaced with fresh media. Afterward, for the

laser-treated group, each well was irradiated with a red laser of 650 nm for 5 min at 50 mW cm^{-2} and further incubated for 24 h. Next, the medium of each well was replaced with 100 μL fresh medium. Then 20 μL freshly prepared MTT solution was incorporated (5 mg mL^{-1}) following a reported method with few alterations.[45] Then after another 4 h of incubation, the media were removed, and 100 μL DMSO was added to dissolve the formed formazan crystal. A microplate reader recorded the absorbance at 570 nm. The cell viability was examined as the ratio of sample absorbance to that of the control.

Evaluation of intracellular reactive oxygen species generation

To evaluate the intracellular reactive oxygen species (ROS) generation, cultured cells (2×10^5 cells per well) were subjected to treatment with DOX, ZnPc, CDs, DOX@CDs, ZnPcPP H, and DOX@CDs–ZnPc-PP H, respectively, for 24 h. In another set of experiments, following treatment with different probes (DOX, ZnPc, CDs, DOX@CDs, ZnPc-PP H, and DOX@CDs–ZnPc-PP H), the cells were irradiated with 650 nm laser at 50 mW cm^{-2} for 5 min. Subsequently, the cells were treated with 10 μM DCFH-DA for 2 h at 37 °C under the dark conditions following a method reported in the literature with some modifications.[31] The treated MCF 7 cells were then washed with PBS buffer along with the subsequent addition of the probes in a 96-well dark plate, and treated cells were subjected to fluorescence measurements at ($\lambda_{ex}/\lambda_{em}$ = 485/528 nm).

Hemocompatibility study of DOX@CDs–ZnPc-PP H

The hemolytic activities of DOX@CDs–ZnPc-PP H were measured using a previously reported method with minor modifications.[72] For this, blood was collected from mice and 1 mL of sodium citrate (3.8% in water) was added, which inhibits the coagulation of blood. Furthermore, 8 mL of blood was centrifuged for 5 minutes at 3000 rpm. RBCs were isolated by decanting supernatant plasma carefully and then washed with PBS (pH 7.4) to obtain only RBC cells. Furthermore, RBCs were redispersed in PBS (pH 7.4) to obtain a uniform cell suspension. Next, different probes, namely, CDs, DOX, ZnPc, DOX@CDs, ZnPcPP H, and DOX@CDs–ZnPc-PP H, respectively, were incubated with RBC cell suspension for 3 h at 37 °C. Only RBCs with PBS are taken as negative control and 1% Triton w/v as a hemolytic agent for positive control. Furthermore, the samples were centrifuged at 3000 rpm for 5 min to collect RBCs. Then, the supernatant was collected from the respective samples to measure the oxidized hemoglobin content. The absorbance of oxyhemoglobin was determined at 540 nm using a UV-Vis spectrophotometer. The percentage of hemolysis of RBCs was estimated using the equation below.

$$\text{Hemolysis}(\%) = \frac{(\text{Abs sample} - \text{Abs negative control})}{(\text{Abs positive control} - \text{Abs negative control})} \times 100 \quad (2)$$

Statistical analysis. A two-way ANOVA was used for the statistical analysis. In this study, data were reported as mean ± SD. The *p*-values of $p < 0.0001$, $^{***}p < 0.001$, $^{**}p < 0.01$, and $^{*}p < 0.05$ were considered statistically significant and ns (non-significant).

Conclusion

In summary, a laser responsive photoarchitectonic hydrogel capable of releasing chemo and photo therapeutic drugs has been developed, to achieve synergistic anticancer therapeutic efficiency. We have reported strategies to develop a unique carrier that integrates DOX-conjugated lignin-based carbon dots and a ZnPc photosensitizer for anticancer therapy. First, we synthesized carbon dots with a size of about 5 nm using lignin and folic acid as biocompatible materials. Following that, doxorubicin (a chemotherapeutic drug) was successfully conjugated into carbon dots with a size of about 12 nm for obtaining DOX@CDs. Subsequently, a laser-responsive hydrogel was developed using zinc phthalocyanine (a photosensitizer), poly(ethylene glycol)methyl ether methacrylate, and PAA. Next, doxorubicin-conjugated carbon dots were added to ZnPc-PP H to form a chemo–phototherapeutic hydrogel (DOX@CDs–ZnPc-PP H). Such a hydrogel triggered the release of chemo and phototherapeutic drugs in response to acidic pH. Furthermore, red laser (650 nm) assisted the release of singlet oxygen from the photosensitizer which acted as a trigger to destroy breast cancer cells. Overall, pH-responsive and laser light-assisted drug release led to *in vitro* cytotoxicity by releasing reactive oxygen species, thus achieving synergistic chemo–photodynamic combinatorial therapy. Importantly, DOX@CDs–ZnPc-PP H, upon stimulation with laser light, generated the highest level of ROS, *i.e.*, 4.5 times higher compared to that of dark treatment. Next, the final combinatorial chemo–photo therapeutic drug exhibited a significant reduction in the cell viability (~50.13% at IC_{50}: 1.06 μg mL^{-1}) in laser treatment compared to dark (IC_{50}: 3.65 μg mL^{-1}). Hence, the newly developed photoarchitectonic hydrogel system with single treatment to cells has shown the highest inhibition rate due to the synergistic effect and hence offers an intriguing concept for successful cancer treatment.

Conflicts of interest

There are no conflicts to declare.

Acknowledgements

All authors are thankful to the Center of Innovative and Applied Bioprocessing (CIAB), the Department of Biotechnology (DBT), Government of India (GOI) for providing funding, infrastructural support, and instrumental facility. J. B. thanks Department of Science and Technology (DST) under Agro-tech scheme for funding support. S. P. acknowledges the CSIR for Fellowship and Regional Centre of Biotechnology, Faridabad, Haryana, for PhD registration. B. Y. acknowledges the DBT for funding and the Regional Centre of Biotechnology, Faridabad, Haryana, for PhD registration. M. D. P. is thankful for the M. K. Bhan fellowship. A. K. P. is grateful for the PhD registration at IISER Mohali.

References

1 R. Dikshit, P. C. Gupta, C. Ramasundarahettige, V. Gajalakshmi, L. Aleksandrowicz, R. Badwe, R. Kumar, S. Roy, W. Suraweera, F. Bray, M. Mallath, P. K. Singh, D. N. Sinha, A. S. Shet, H. Gelband and P. Jha, *Lancet*, 2012, **379**, 1807–1816.

2 D. Hanahan and R. A. Weinberg, *Cell*, 2011, **144**, 646–674.

3 J. Ferlay, E. Steliarova-Foucher, J. Lortet-Tieulent, S. Rosso, J. W. W. Coebergh, H. Comber, D. Forman and F. Bray, *Eur. J. Cancer*, 2013, **49**, 1374–1403.

4 S. Paul, P. P. Solanki, U. P. Shahi and S. Srikrishna, *Asian Pac. J. Cancer Prev.*, 2016, **16**, 8163–8171.

5 R. L. Siegel, K. D. Miller, H. E. Fuchs and A. Jemal, *Ca-Cancer J. Clin.*, 2021, **71**, 7–33.

6 L. Yang, Z. Wang, J. Wang, W. Jiang, X. Jiang, Z. Bai, Y. He, J. Jiang, D. Wang and L. Yang, *Nanoscale*, 2016, **8**, 6801–6809.

7 J. R. McCarthy, J. Bhaumik, M. R. Karver, S. Sibel Erdem and R. Weissleder, *Mol. Oncol.*, 2010, **4**, 511.

8 M. D. Patil, J. Bhaumik, S. Babykutty, U. C. Banerjee and D. Fukumura, *Oncogene*, 2016, **35**, 4957–4972.

9 Z. Chen, X. Wang, Y. Ding, C. Xing, C. Lu and X. Tu, *ACS Mater. Lett.*, 2023, 1237–1244.

10 A. M. Bugaj, *Photochem. Photobiol. Sci.*, 2011, **10**, 1097–1109.

11 S. N. Baker and G. A. Baker, *Angew. Chem., Int. Ed.*, 2010, **49**, 6726–6744.

12 M. Zheng, S. Liu, J. Li, D. Qu, H. Zhao, X. Guan, X. Hu, Z. Xie, X. Jing and Z. Sun, *Adv. Mater.*, 2014, **26**, 3554–3560.

13 H. Liu, T. Ye, C. Mao, H. Liu, T. Ye and C. Mao, *Angew. Chem., Int. Ed.*, 2007, **46**, 6473–6475.

14 A. Sachdev and P. Gopinath, *Analyst*, 2015, **140**, 4260–4269.

15 W. R. Zhuang, Y. Wang, P. F. Cui, L. Xing, J. Lee, D. Kim, H. L. Jiang and Y. K. Oh, *J. Controlled Release*, 2019, **294**, 311–326.

16 Y. Chen, L. Zhang, F. Li, J. Sheng, C. Xu, D. Li, H. Yu and W. Liu, *Int. J. Nanomed.*, 2021, **16**, 3679.

17 Y. Zhang, F. Huang, C. Ren, L. Yang, J. Liu, Z. Cheng, L. Chu and J. Liu, *ACS Appl. Mater. Interfaces*, 2017, **9**, 13016–13028.

18 M. Yu, J. Yu, Y. Yi, T. Chen, L. Yu, W. Zeng, X. Kun Ouyang, C. Huang, S. Sun, Y. Wang, Y. Liu, C. Lin, M. Wu and L. Mei, *J. Controlled Release*, 2022, **347**, 104–114.

19 Z. Li, Y. Yang, H. Wei, X. Shan, X. Wang, M. Ou, Q. Liu, N. Gao, H. Chen, L. Mei and X. Zeng, *J. Controlled Release*, 2021, **338**, 719–730.

20 Q. Liu, L. Yang, L. Wang, Z. Li, Y. Yu, Y. Zheng, D. Lian, X. Li, H. Chen, L. Mei, X. Zeng and N. Gao, *Int. J. Biol. Macromol.*, 2023, **244**, 125064.

21 H. Chen, T. Sun, W. Zeng, X. Zeng, L. Mei, C. Jiang and Y. Zhao, *ACS Mater. Lett.*, 2022, **4**, 111–119.

22 Y. Yang, W. Zeng, P. Huang, X. Zeng and L. Mei, *View*, 2020, 20200042.

23 C. Hongzhong, *Angew. Chem., Int. Ed.*, 2019, **58**(23), 7641–7646.

24 J. Zhai, H. Yang, Z. Wang, Y. Li and C. Ning, *Smart Mater. Med.*, 2022, **3**, 315–328.

25 G. Saravanakumar, J. Kim and W. J. Kim, *Adv. Sci.*, 2016, 1600124.

26 S. Paul, N. S. Thakur, S. Chandna, Y. N. Reddy and J. Bhaumik, *J. Mater. Chem. B*, 2021, **9**, 1592–1603.

27 S. Paul, N. S. Thakur, S. Chandna, V. Sagar and J. Bhaumik, *ACS Appl. Nano Mater.*, 2022, **5**, 2748–2761.

28 T. D. De Souza, F. I. Ziembowicz, D. F. Müller, S. C. Lauermann, C. L. Kloster, R. C. V. Santos, L. Q. S. Lopes, A. F. Ourique, G. MacHado and M. A. Villetti, *Eur. J. Pharm. Sci.*, 2016, **83**, 88–98.

29 F. N. Velazquez, M. Miretti, M. T. Baumgartner, B. L. Caputto, T. C. Tempesti and C. G. Prucca, *Sci. Rep.*, 2019, **9**, 1–15.

30 C. Liang, X. Zhang, M. Yang, W. Wang, P. Chen and X. Dong, *ACS Mater. Lett.*, 2020, **2**, 1268–1286.

31 N. S. Thakur, N. Mandal, G. Patel, S. Kirar, Y. N. Reddy, V. Kushwah, S. Jain, Y. N. Kalia, J. Bhaumik and U. C. Banerjee, *Nanomedicine*, 2021, **33**, 102368.

32 C. Fabris, M. Soncin, G. Miotto, L. Fantetti, G. Chiti, D. Dei, G. Roncucci and G. Jori, *J. Photochem. Photobiol., B*, 2006, **83**, 48–54.

33 I. M. Tynga, N. N. Houreld and H. Abrahamse, *J. Photochem. Photobiol., B*, 2013, **120**, 171–176.

34 W. Chidawanyika, A. Ogunsipe and T. Nyokong, *New J. Chem.*, 2007, **31**, 377–384.

35 S. Chandna, S. Paul, R. Kaur, K. Gogde and J. Bhaumik, *ACS Appl. Polym. Mater.*, 2022, **4**, 8962–8976.

36 Z. Li, L. Yang, D. Zhang, W. Wang, Q. Huang, Q. Liu, K. Shi, Y. Yu, N. Gao, H. Chen, S. Jiang, Z. Xie and X. Zeng, *J. Colloid Interface Sci.*, 2023, **650**, 1907–1917.

37 Y. Liu, M. Zhu, M. Meng, Q. Wang, Y. Wang, Y. Lei, Y. Zhang, L. Weng and X. Chen, *Chin. Chem. Lett.*, 2023, **34**(1), 107583.

38 F. M. Chen and X. Liu, *Prog. Polym. Sci.*, 2016, **53**, 86.

39 C. Martín, A. Bachiller, J. P. Fernández-Blázquez, Y. Nishina and J. L. Jorcano, *ACS Mater. Lett.*, 2023, **5**, 1245–1255.

40 Y. N. Reddy, A. De, S. Paul, A. K. Pujari and J. Bhaumik, *Biomacromolecules*, 2023, **24**(4), 1717–1730.

41 Y. Zhao, C. Shi, X. Yang, B. Shen, Y. Sun, Y. Chen, X. Xu, H. Sun, K. Yu, B. Yang and Q. Lin, *ACS Nano*, 2016, **10**, 5856–5863.

42 N. K. Singh, Q. V. Nguyen, B. S. Kim and D. S. Lee, *Nanoscale*, 2015, **7**, 3043–3054.

43 J. Girón-Hernández, P. Gentile and M. Benlloch-Tinoco, *Carbohydr. Polym.*, 2021, **271**, 118429.

44 S. I. Ali, J. P. A. Heuts and A. M. Van Herk, *Soft Matter*, 2011, **7**, 5382–5390.

45 X. Chen, X. Zhang, Y. Guo, Y. X. Zhu, X. Liu, Z. Chen and F. G. Wu, *Adv. Funct. Mater.*, 2019, **29**, 1807772.

46 Z. Sun, C. Song, C. Wang, Y. Hu and J. Wu, *Mol. Pharmaceutics*, 2020, **17**, 373–391.

47 J. Ma, B. Wang, H. Shao, S. Zhang, X. Chen, F. Li and W. Liang, *Drug Delivery*, 2022, **29**, 1457–1476.

48 A. P. Singh, A. Biswas, A. Shukla and P. Maiti, *Signal Transduction Targeted Ther.*, 2019, **4**, 1–21.

49 A. Pal, M. P. Sk and A. Chattopadhyay, *Mater. Adv.*, 2020, **1**, 525–553.

50 S. Zhu, Q. Meng, L. Wang, J. Zhang, Y. Song, H. Jin, K. Zhang, H. Sun, H. Wang and B. Yang, *Angew. Chem., Int. Ed.*, 2013, **125**, 4045–4049.
51 S. Rai, B. K. Singh, P. Bhartiya, A. Singh, H. Kumar, P. K. Dutta and G. K. Mehrotra, *J. Lumin.*, 2017, **190**, 492–503.
52 A. Mewada, S. Pandey, M. Thakur, D. Jadhav and M. Sharon, *J. Mater. Chem. B*, 2014, **2**, 698–705.
53 W. Kuzyniak, J. Schmidt, W. Glac, J. Berkholz, G. Steinemann, B. Hoffmann, E. A. Ermilov, A. G. Görek, V. Ahsen, B. Nitzsche and M. Höpfner, *Int. J. Oncol.*, 2017, **50**, 953–963.
54 C. Chen, G. Chu, M. Qi, Y. Liu, P. Huang, H. Pan, Y. Wang, Y. Chen and Y. Zhou, *ACS Appl. Bio Mater.*, 2020, **3**, 9117–9125.
55 B. Tran, I. O. Oladeji, J. Zou, G. Chai and L. Zhai, *Solid State Ionics*, 2013, **232**, 37–43.
56 J.-O. Jeong, J. Baik, S.-J. An, S.-I. Jeong, J.-Y. Lee, Y.-M. Lim and J.-S. Park, *arXiv*, 2018, preprint, 2018010028, DOI: **10.20944/preprints201801.0028.v1**.
57 J. Janczak, *Polyhedron*, 2020, **178**, 114313.
58 K. Zhu, C. Wang, J. Liu, W. Wang, Y. Lv, P. Wang, A. Meng and Z. Li, *J. Australas. Ceram. Soc.*, 2020, **8**, 939–947.
59 S. K. Swain and K. Prusty, *J. Mater. Sci.*, 2017, **53**, 2303–2325.
60 P. Khomein, A. Nallapaneni, J. Lau, D. Lilley, C. Zhu, S. Kaur, R. Prasher and G. Liu, *Sol. Energy Mater. Sol. Cells*, 2021, **225**, 111030.
61 C. Trujillo and G. Sánchez-Sanz, *ChemPhysChem*, 2016, **17**, 395–405.
62 M. Zhou, S. Liu, Y. Jiang, H. Ma, M. Shi, Q. Wang, W. Zhong, W. Liao and M. M. Q. Xing, *Adv. Funct. Mater.*, 2015, **25**, 4730–4739.
63 X. Chen, Z. Song, S. Li, N. Tat Thang, X. Gao, X. Gong and M. Guo, *Green Chem.*, 2020, **22**, 3296–3308.
64 G. Guedes, S. Wang, F. Fontana, P. Figueiredo, J. Lindén, A. Correia, R. J. B. Pinto, S. Hietala, F. L. Sousa, H. A. Santos, G. Guedes, S. Wang, F. Fontana, P. Figueiredo, A. Correia, H. A. Santos, R. J. B. Pinto and F. L. Sousa, *Adv. Mater.*, 2021, **33**, 2007761.
65 L. E. Kass and J. Nguyen, *Wiley Interdiscip. Rev.: Nanomed. Nanobiotechnol.*, 2022, **14**, e1756.
66 W. Qing, X. Xing, D. Feng, R. Chen and Z. Liu, *Photodiagn. Photodyn. Ther.*, 2021, **36**, 102521.
67 Y. Zhou, C. Chang, Z. Liu, Q. Zhao, Q. Xu, C. Li, Y. Chen, Y. Zhang and B. Lu, *Langmuir*, 2021, **37**, 2619–2628.
68 B. Yang, Y. Chen and J. Shi, *Chem. Rev.*, 2019, **119**, 4881–4985.
69 Y. N. Reddy, S. Kirar, N. S. Thakur, M. D. Patil and J. Bhaumik, *ACS Sustainable Chem. Eng.*, 2023, **11**, 12.
70 K. Gogde, S. Paul, A. K. Pujari, A. K. Yadav and J. Bhaumik, *J. Med. Chem.*, 2023, **66**(18), 13058–13071.
71 K. Lin, Y. Rong, D. Chen, Z. Zhao, H. Bo, A. Qiao, X. Hao and J. Wang, *Front. Oncol.*, 2020, **10**, 141.
72 K. Jadhav, S. Deore, D. Dhamecha, R. Hr, S. Jagwani, S. Jalalpure and R. Bohara, *ACS Biomater. Sci. Eng.*, 2018, **4**, 892–899.
73 V. R. Muzykantov, *Expert Opin. Drug Delivery*, 2010, **7**, 403.
74 G. Rukh, A. Ullah, R. Khattak, P. Fazil, A. Ali, M. R. Shah, M. S. Khan, A. S. Alsubaie, K. H. Mahmoud and M. Ateeq, *Coatings*, 2022, **12**, 200.
75 N. S. Thakur, G. Patel, V. Kushwah, S. Jain and U. C. Banerjee, *ACS Appl. Bio Mater.*, 2019, **2**, 349–361.